

Equatorial zonal electric fields inferred from a 3-D electrostatic potential model and ground-based magnetic field measurements

E. B. Shume,¹ E. R. de Paula,¹ S. Maus,² D. L. Hysell,³ F. S. Rodrigues,⁴ and A. Bekele⁵

Received 10 February 2009; revised 25 March 2009; accepted 31 March 2009; published 6 June 2009.

[1] We present a new technique to infer quiet time zonal electric fields in the daytime equatorial ionosphere. The electric field inference technique utilizes a three-dimensional (3-D) electrostatic potential model of the low-latitude ionosphere constrained by ground-based magnetic field measurements. To test this technique, inferred zonal electric fields for the Peruvian sector in Jicamarca (11.95°S, 283.13°E, 0.6°N dip latitude) were compared with zonal electric field (vertical drift) measurements made by the Jicamarca Incoherent Scatter Radar. The comparison shows a good agreement between the inferred and measured electric fields. An example of electric field estimation for Davao (7.4°N, 125.4°E, 0.58°S dip latitude) in the Philippines sector is also presented in this report. Inferred electric fields for Davao are in good agreement with F region vertical plasma drifts measured by drift sensors onboard the AE-E and ROCSAT-1 satellites on that longitude sector. Our results suggest that realistic estimates of quiet time zonal electric fields for the equatorial ionosphere can be obtained from the 3-D potential model whenever observatory magnetic field measurements are available.

Citation: Shume, E. B., E. R. de Paula, S. Maus, D. L. Hysell, F. S. Rodrigues, and A. Bekele (2009), Equatorial zonal electric fields inferred from a 3-D electrostatic potential model and ground-based magnetic field measurements, *J. Geophys. Res.*, *114*, A06305, doi:10.1029/2009JA014158.

1. Introduction

[2] Equatorial zonal electric fields control vertical plasma transport in the low-latitude ionosphere [Kelley, 1989; Fejer, 1997]. It drives the equatorial electrojet and the equatorial ionization anomalies [Rush and Richmond, 1973; Kelley, 1989]. During the evening, it drives plasma to higher altitudes increasing the linear instability growth rate of spread F plasma instabilities [Kelley, 1989; Sultan, 1996].

[3] Zonal electric fields of the equatorial ionosphere have been routinely measured utilizing the 50 MHz Incoherent Scatter Radar (ISR) in Jicamarca, Perú [Woodman, 1970; Balsley, 1973; Fejer et al., 1991; Fejer, 1997]. Consequently, the diurnal, seasonal, and solar cycle dependence of the equatorial zonal electric fields have been extensively investigated in the South American (West coast) longitude sector [Fejer et al., 1979, 1989, 1991]. The Jicamarca Unattended Long-term Investigations of the Ionosphere and Atmosphere (JULIA) coherent scatter radar at

Jicamarca, which utilizes nonthermal scattering from the equatorial electrojet and 150-km echo plasma irregularities, has been also employed to estimate equatorial zonal electric fields [Hysell et al., 1997; Hysell and Burcham, 2000; Chau and Woodman, 2004]. AE-E and ROCSAT-1 satellite missions have been instrumental for studying the longitudinal dependence of averaged zonal electric fields of the equatorial ionosphere [Fejer et al., 1995, 2008]. However, day-to-day monitoring of the characteristics of the equatorial zonal electric field in longitude sectors other than the West coast of South America has not been forthcoming.

[4] Vertical $\mathbf{E} \times \mathbf{B}$ drift velocities of the daytime equatorial ionosphere have been inferred from ground-based magnetometer observations [Anderson et al., 2002, 2004, 2006]. The technique of Anderson et al. [2002, 2004] establishes empirical relationships between the strength of the daytime equatorial electrojet current and the vertical F region $\mathbf{E} \times \mathbf{B}$ drift velocity in the South American (West coast) sector. Anderson et al. [2006] have also used a neural network algorithm, which was trained in the Peruvian sector, to infer vertical drift velocities in the Philippines longitude sector.

[5] Using the NCAR Thermosphere Ionosphere Electrodynamics General Circulation Model (TIE GCM), Fang et al. [2008a] have calculated equatorial magnetic field perturbations and ionospheric vertical plasma drifts. Their model calculation has mainly captured the diurnal, seasonal, and solar activity dependence of magnetic field perturbations in the Peruvian and the Philippines longitudes sectors.

¹National Institute for Space Research, São José dos Campos, Brazil.

²National Geophysical Data Center, NOAA, Boulder, Colorado, USA.

³Department of Earth and Atmospheric Sciences, Cornell University, Ithaca, New York, USA.

⁴Atmospheric and Space Technology Research Associates, San Antonio, Texas, USA.

⁵Department of Physics, Addis Ababa University, Addis Ababa, Ethiopia.

[6] Numerical models using simplifying two-dimensional (2-D) geometries to relate the eastward electric field to the strength of the equatorial electrojet have been developed by *Sugiura and Poros* [1969], *Richmond* [1973b], and *Maus et al.* [2007]. In the present work, we use a full three-dimensional (3-D) electrostatic potential model to infer quiet time zonal electric fields in the daytime equatorial ionosphere from ground-based magnetic field perturbation estimates. The 3-D potential model has been previously used by *Hysell et al.* [2002], *Shume et al.* [2005b], and *Shume* [2006] for investigating zonal wind profiles in the equatorial ionosphere. Constrained by ground-based magnetic field perturbation measurements, the 3-D physics-based computational model predicts electric field and current density vectors through out the low-latitude ionosphere. The potential model infers zonal electric fields in an iterative fashion. The strategy we have employed in the inference is to tune up the zonal electric fields in the model for optimal agreement between the modeled and measured magnetic field perturbation estimates.

[7] Section 2 describes the method of estimating ground-based magnetic field perturbations, a measure of the electrojet strength. A brief description of the 3-D electrostatic potential model employed in this study is presented in section 3. Temporal properties of inferred zonal electric fields for daytime equatorial ionosphere in the Peruvian and the Philippines longitude sectors are presented and discussed in section 4. Section 5 summarizes this report.

2. Ground-Based Magnetic Field Measurements

[8] The strength of the equatorial electrojet is commonly measured by ground-based magnetometers located at equatorial stations. ΔH_m , which is a measure of the strength of the equatorial electrojet, can be obtained by calculating the difference in magnitude of the measured horizontal magnetic field component between a magnetometer placed on the magnetic equator and one placed $6^\circ - 9^\circ$ away [Anderson et al., 2002, 2004, 2006]. Accordingly, horizontal magnetic field residues ΔH_m at Jicamarca, Perú, (11.95°S , 283.13°E , 0.6°N dip latitude) are obtained by subtracting from it magnetic field measurements at Piura, Perú (5.11°S , 80.34°W , 6.67°N). Nighttime baseline magnetometer records for each station are subtracted first to obtain daytime values. We have used similar procedures to determine ΔH_m at Davao, the Philippines (7.4°N , 125.4°E , 0.58°S dip latitude) using off-dip-equator data from a magnetometer placed at Muntinlupa, the Philippines, (14.4°N , 121.0°E , 6.79°N). The 3-D electrostatic potential model approach described in the next section reproduces ΔH_m by modeling the equatorial electrojet, thereby inferring zonal electric fields.

3. Potential Model

[9] Current density \mathbf{J} in the ionosphere can be described as [Forbes, 1981]

$$\mathbf{J} = \hat{\Sigma} \cdot (\mathbf{E} + \mathbf{U} \times \mathbf{B}) \quad (1)$$

where $\hat{\Sigma}$ is a second-order conductivity tensor, \mathbf{E} is an electric field, \mathbf{U} is the neutral wind velocity, and \mathbf{B} is the

geomagnetic field. Elements of the conductivity tensor are function of the Pedersen σ_P , Hall σ_H , and parallel σ_\parallel conductivities. Mathematical definitions of the conductivities are given by *Forbes* [1981] and *Kelley* [1989], for example.

[10] The electric field \mathbf{E} can be resolved into a background (dawn-dusk) electric field component \mathbf{E}_\circ and a perturbed electric field component $-\nabla\Phi$, where Φ is an electrostatic potential:

$$\mathbf{E} = \mathbf{E}_\circ - \nabla\Phi \quad (2)$$

As long as current driven by the background electric field \mathbf{E}_\circ and neutral winds $\mathbf{U} \times \mathbf{B}$ are divergent, the electric field $-\nabla\Phi$ is established to maintain divergence-free current in the ionosphere $\nabla \cdot \mathbf{J} = 0$ giving rise to the second-order potential equation

$$\nabla \cdot (\hat{\Sigma} \cdot \nabla\Phi) = \nabla \cdot [\hat{\Sigma} \cdot (\mathbf{E}_\circ + \mathbf{U} \times \mathbf{B})] \quad (3)$$

[11] We seek solution of the second-order nonhomogeneous partial differential equation (3) in the low-latitude ionosphere, utilizing the multigrid method described by *Shume et al.* [2005b], in a magnetic dipole coordinates (p , q , φ) [Hysell et al., 2004; Shume et al., 2005b]. The magnetic dipole coordinates (p , q , φ) are perpendicular upward, parallel to \mathbf{B} , and perpendicular eastward, respectively. Neumann boundary conditions are imposed on the q , φ , and lower p boundaries, and on the upper p boundary, the perturbed electric fields are set assuming a perfectly efficient wind driven dynamo.

[12] Our simulation spaces are the low-latitude ionosphere in (1) the Peruvian longitude sector centered at Jicamarca (11.95°S , 283.13°E ; 0.6°N dip latitude) and (2) the Philippines longitude sector centered at Davao (7.4°N , 125.4°E , 0.58°S dip latitude). The solution space contains 73, 73, and 37 grid points in the (p , q , φ) coordinates, respectively. It covers between 85 to 150 km of altitude and is $\pm 10^\circ$ wide both in latitude and longitude.

[13] Input ionospheric parameters used in the model calculations: Plasma conductivities were calculated using neutral atmosphere densities and temperatures derived from the Mass Spectrometer Incoherent Scatter (MSIS-E-90) model [Hedin, 1991], plasma density and ionospheric composition estimates from the International Reference Ionosphere (IRI) model specification [Bilitza, 2001], geomagnetic field information from the International Geomagnetic Reference Field (IGRF) model [Maus et al., 2005], and empirical collision frequencies were taken from *Nicolet* [1953], *Richmond* [1972], and *Gagnepain et al.* [1977]. Since the IRI model overestimates electron densities below the E region peak, electron density profiles derived from an α Chapman function is employed there [Shume et al., 2005a, 2005b]. This procedure gives rise to a fairly accurate representation of the E region plasma density profiles for our numerical model runs. Our potential model run made use of zonal neutral wind velocities derived from the Horizontal Wind Model (HWM) [Hedin et al., 1996].

[14] The potential model runs are then performed in such a way that equatorial zonal electric fields are inferred in an iterative fashion: model runs are repeated by readjusting the

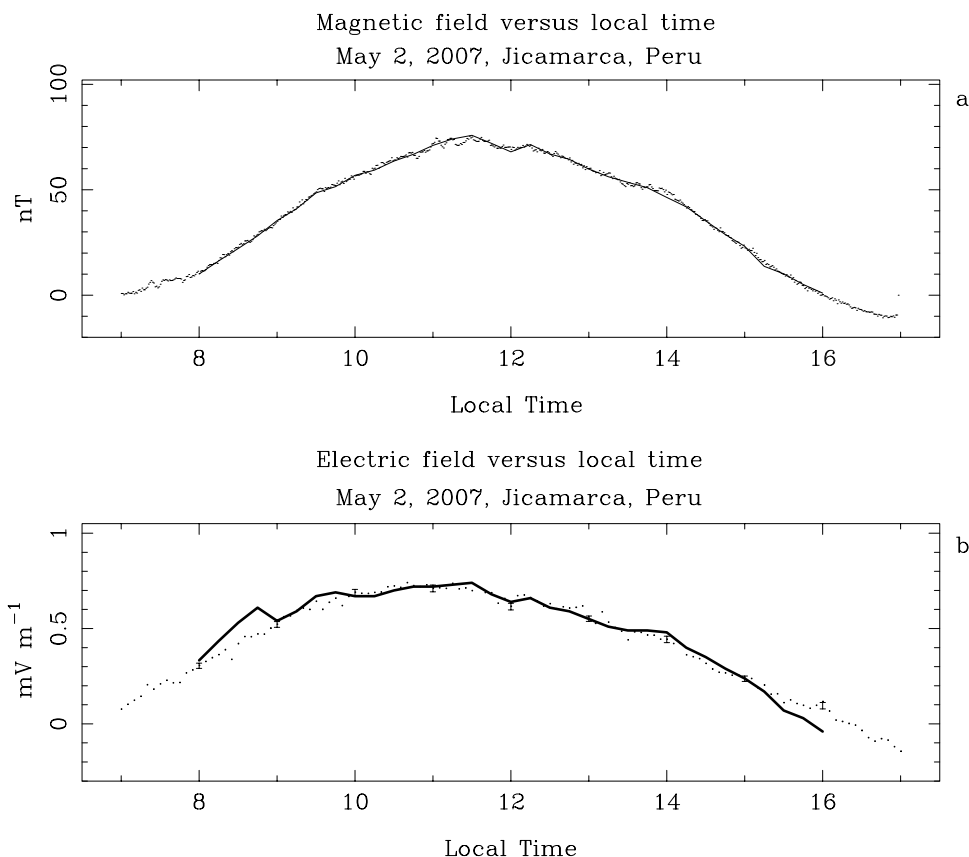


Figure 1. (a) Measured (dots) and modeled (solid line) horizontal magnetic field perturbations in the Peruvian sector over Jicamarca (2 May 2007). (b) Measured (dots) and calculated (thick solid line) zonal electric fields over Jicamarca, Perú. The error bars of zonal electric field measurements are also shown.

zonal electric field in the model until the measured magnetic field perturbations ΔH_m are reproduced.

4. Results and Discussion

4.1. Inferred Zonal Electric Fields: Jicamarca, Perú

[15] Figure 1a shows the temporal variation of the magnetic field perturbation ΔH_m measured at Jicamarca (dots), and the magnetic field perturbation ΔH_c estimated using the potential model runs (solid line) on 2 May 2007. This day can be considered as geomagnetically quiet ($a_p < 10$). For this model run, the center of the simulation space was located at Jicamarca, Perú. The potential model was run in quarter of an hour interval from 0800 to 1600 Local Time (LT) for geophysical conditions representative of 2 May 2007. Model runs were carried out by making an initial guess for the background electric field \mathbf{E}_0 and modifying the guess until ΔH_c comes to a close agreement with ΔH_m as illustrated in Figure 1a. Figure 1a shows that the model calculations ΔH_c capture well the time evolution of ΔH_m for all time steps. Figure 1a also shows that both the measured and calculated perturbed magnetic fields have peaks around 1130 LT with $\Delta H_m = 75.0$ nT and $\Delta H_c = 75.8$ nT. A maximum difference between ΔH_m and ΔH_c of about 0.9 nT can be seen around 1100 LT.

[16] Figure 1b shows the zonal electric field estimated from the model (thick solid line) and zonal electric field

measured at Jicamarca (dots) as a function of local time. The modeled electric field shown corresponds to 150 km altitude in the simulation space. The measured electric field and error bars were obtained from F region $\mathbf{E} \times \mathbf{B}$ plasma drifts measured by the Jicamarca ISR averaged around 220 km altitude. Note that when running in ISR mode, the Jicamarca radar cannot measure drifts below 200 km owing to clutter from the equatorial electrojet contaminating incoherent scatter echoes. Average ISR vertical drifts during the day, however, are in good agreement with vertical drifts from the so-called 150-km echo plasma irregularities at Jicamarca [Chau and Woodman, 2004]. Balsley and Woodman [1969] and Woodman [1970] also suggested a close relationship between electric fields that drive the equatorial electrojet and electric fields that produce F region vertical plasma drifts in the equatorial ionosphere.

[17] Figure 1b has shown that with the exception of around 0845 LT and 1600 LT, the agreement between the inferred and measured zonal electric field time series are good. Around these two local times, the measured electric fields were 0.47 mV m^{-1} and 0.095 mV m^{-1} , respectively. The calculated electric fields, on the other hand, are 0.61 mV m^{-1} and -0.04 mV m^{-1} , respectively. The largest difference between the two electric field estimates is about 0.14 mV m^{-1} and occurs around 0845 LT.

[18] The time when the equatorial electrojet strength reaches its maximum (Figure 1a) coincides with the time

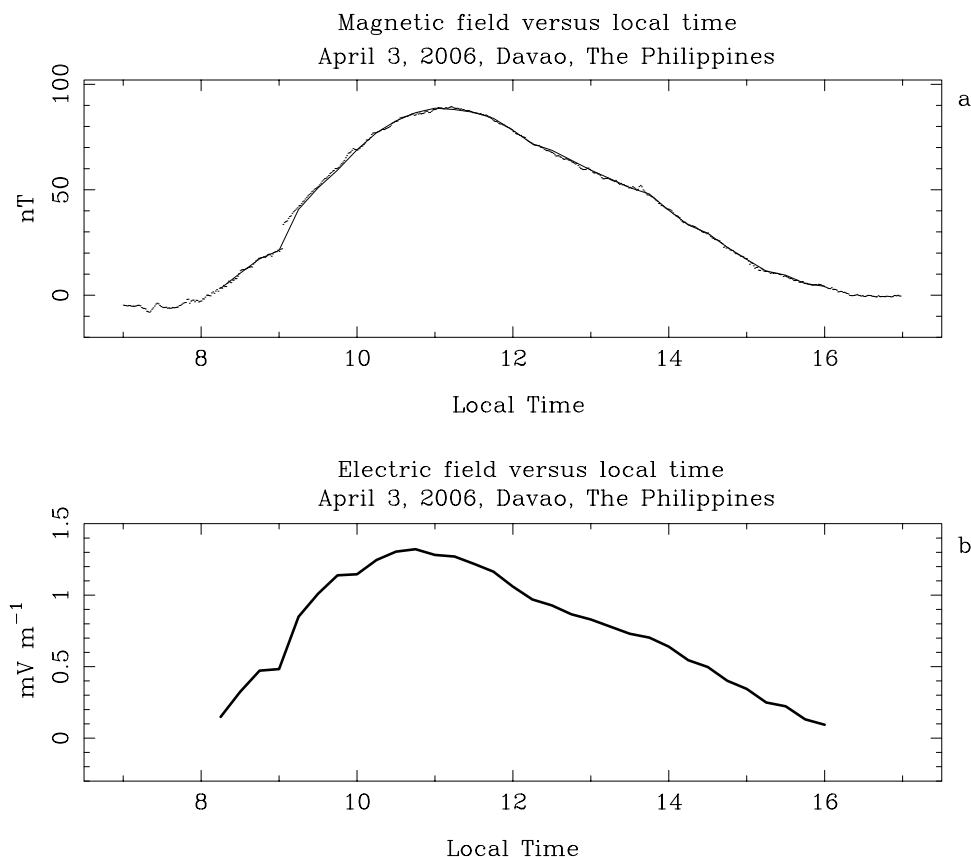


Figure 2. (a) Same as Figure 1a but for the Philippines sector over Davao (2 April 2006). (b) Temporal variation of the calculated zonal electric field over Davao, the Philippines are shown by thick solid line.

when the zonal electric field reaches its peak (Figures 1b), confirming the finding of *Balsley and Woodman* [1969] and *Anderson et al.* [2002]. The maximum values happen to occur around 1130 LT.

4.2. Inferred Zonal Electric Fields: Davao, The Philippines

[19] We have carried out a similar analysis for the Philippines longitude sector in Davao (center of simulation space for this model run). Model results are shown in Figure 2.

[20] Figure 2a shows a comparison between the measured (dots) ΔH_m and calculated (solid line) ΔH_c magnetic field perturbations over Davao, the Philippines on 3 April 2006. This day again can be considered as a geomagnetically quiet day ($a_p < 10$). Figure 2a again shows that the agreement between the two magnetic field perturbation estimates, ΔH_c and ΔH_m , is very good.

[21] Time series of zonal electric field generated by the potential model run is shown in Figure 2b. Around 1100 LT, the zonal electric field estimated by the model run becomes as large as 1.30 mV m^{-1} . The magnitude of the modeled zonal electric field for Davao was compared with F region vertical $\mathbf{E} \times \mathbf{B}$ plasma drifts measured by the Ion Drift Meter (IDM instrument) onboard the AE-E satellite and by the Ionospheric Plasma and Electrodynamics Instrument (IPEI) onboard the ROCSAT-1 satellite during equinox seasons [*Fejer et al.*, 1995, 2008]. The zonal electric field producing the vertical plasma drifts seen by these two

satellites is in the range between 1.28 and 1.64 mV m^{-1} around 1100 LT. These values are in good agreement with the modeled zonal electric field ($\sim 1.30 \text{ mV m}^{-1}$) around 1100 LT on 3 April 2006.

4.3. Sensitivity Analysis

4.3.1. Zonal Neutral Winds

[22] In order to study the effects of zonal winds on the zonal electric field (and its temporal properties), we have carried out model runs over Jicamarca (2 May 2007) by turning off the zonal winds. Figure 3a shows a comparison between zonal electric fields calculated (thin solid line) from model runs by turning off the zonal winds, zonal electric fields calculated (thick solid line) when zonal winds are turned on, and zonal electric fields measured by the Jicamarca ISR (dots). The difference between the calculated electric fields with and without winds can be as large as 0.15 mV m^{-1} (around 1600 LT).

[23] Figure 3a shows that the calculated electric field from model runs with zonal winds turned off generally underestimate the measured electric fields before about 1200 LT. However, zonal electric fields calculated from zero-wind model runs generally overestimate the measured electric field after about 1200 LT. These results suggest that wind dynamos contribute negatively to magnetic field perturbations and zonal electric fields before about 1200 LT and positively after about 1200 LT. The modulating effect of wind dynamos on ground magnetic field perturbations and zonal electric fields have been shown by *Fang et*

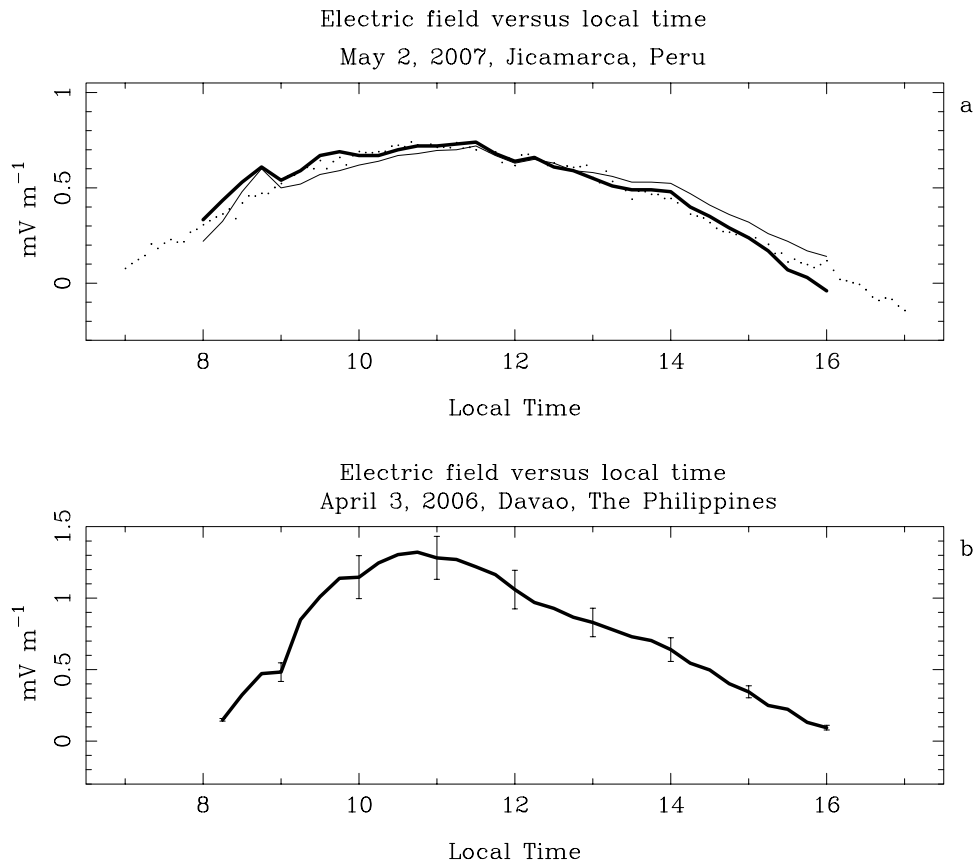


Figure 3. (a) Modeled electric fields in the absence (thin solid line) and presence (thick solid line) of zonal winds over Jicamarca, Perú. (b) Modeled electric fields over Davao, the Philippines. The effect of variation of electron density profiles on inferred zonal electric fields are shown by error bars.

al. [2008b]. Zonal winds also contribute in determining the latitudinal distribution of the ionospheric current system [Hysell *et al.*, 2002; Fang *et al.*, 2008b]. Zonal winds, however, have a marginal role in driving the equatorial electrojet (or causing magnetic field perturbations) and generating zonal electric fields in the electrojet region [Richmond, 1973a; Reddy and Devasia, 1981; Hysell *et al.*, 2002; Fang *et al.*, 2008b].

4.3.2. Electron Densities

[24] As mentioned in section 3, to provide a fairly accurate electron density profiles for our model calculations, we have used a combination of electron density profiles derived from an α Chapman function with the IRI model plasma density profiles. Chapman density profiles were found out to be in a very good agreement with E region electron density profiles measured by a bistatic coherent scatter radar at Jicamarca (and Piura, Perú) [Shume *et al.*, 2005a, Figure 1b]. These density profiles were also used as input by Shume *et al.* [2005b] to model zonal wind profiles in the equatorial electrojet region.

[25] Here, we have shown the effect of variation of electron density profiles employed in the research (section 4.2) on the modeled zonal electric fields. Model runs were conducted over Davao (3 April 2006) by varying the density profiles by $\pm 10\%$. The uncertainties of zonal electric fields due to these changes in density profiles are shown by error bars in Figure 3b. The electric field time

series shown in Figure 3b is identical to those shown in Figure 2b. The largest and smallest error bars were about $1.28 \pm 0.16 \text{ mV m}^{-1}$ and $0.092 \pm 0.01 \text{ mV}^{-1}$, and occurred at about 1100 and 0800 LT, respectively.

5. Summary and Conclusion

[26] Zonal electric fields of the equatorial ionosphere are mainly responsible for driving the equatorial electrojet and the equatorial ionization anomalies. Zonal electric field during evening hours drives plasma to higher altitudes thereby creating suitable conditions for equatorial spread F plasma instabilities to occur. Knowledge of equatorial zonal electric fields is vital for understanding plasma dynamics of the equatorial and low-latitude ionosphere.

[27] We have reported results of a new technique to infer quiet time zonal electric fields in the daytime equatorial ionosphere. The electric field inference technique is based on a 3-D electrostatic potential computational model for the low-latitude ionosphere constrained by ground-based magnetic field perturbation measurements. The 3-D physics-based numerical model calculates electric field and the strength of equatorial electrojet current. The zonal electric field inference was done iteratively: the zonal electric field is tuned up in the model until modeled magnetic field perturbations match the measurements.

[28] We have shown that inferred zonal electric fields for Jicamarca, Perú are in good agreement with zonal electric

fields estimated from vertical plasma drifts measured by the Jicamarca ISR. The electric field inference technique has also been applied to infer zonal electric field over Davao, the Philippines. The inferred zonal electric field over Davao is in good agreement with F region vertical plasma drift velocities measured by IDM and IPEI drift sensors onboard AE-E and ROCSAT-1 satellites, respectively. Our results suggest that the electric field inference technique can be applied to infer zonal electric fields in other longitude sectors whenever observatory magnetic field measurements are available.

[29] In the near future, the 3-D electrostatic potential model approach employed in this research will be applied to model and investigate characteristics of equatorial zonal electric fields during geomagnetic storm conditions. Zonal electric fields derived from the potential model will be also utilized to study longitudinal and seasonal variabilities of the equatorial electrojet and electrodynamics of the equatorial ionosphere.

[30] **Acknowledgments.** E. Shume is supported by FAPESP under process number 2007/08185-9 at INPE. E. Shume thanks the World Data Center for Geophysics and Marine Geology, Boulder Visiting Scientist Program, for funding his visit to NOAA/National Geophysical Data Center (NGDC), Boulder, Colorado, in July–August 2008. The Jicamarca Radio Observatory is a facility of the Instituto Geofísico del Perú operated with support from the NSF Cooperative Agreement ATM-0432565 through Cornell University. Magnetometer data for Davao and Muntinlupa stations (the Philippines) were obtained from MAGDAS, the Space Environment Research Center, Kyushu University, Japan. The MUDPACK package used for this research (copyright John C. Adams) was obtained from UCAR which is sponsored by the NSF. The authors would like to thank the constructive comments given by one of the anonymous reviewers.

[31] Wolfgang Baumjohann thanks Michael Nicolls and another reviewer for their assistance in evaluating this paper.

References

- Anderson, D., A. Anghel, K. Yumoto, and M. Ishitsuka (2002), Estimating daytime vertical $\mathbf{E} \times \mathbf{B}$ drift velocities in the equatorial F region using ground-based magnetometer observations, *Geophys. Res. Lett.*, *29*(12), 1596, doi:10.1029/2001GL014562.
- Anderson, D., A. Anghel, J. Chau, and O. Veliz (2004), Daytime vertical $\mathbf{E} \times \mathbf{B}$ drift velocities inferred from ground-based magnetometer observations at the low latitudes, *Space Weather*, *2*, S11001, doi:10.1029/2004SW000095.
- Anderson, D., A. Anghel, J. L. Chau, and K. Yumoto (2006), Global, low-latitude, vertical $\mathbf{E} \times \mathbf{B}$ drift velocities inferred from daytime magnetometer observations, *Space Weather*, *4*, S08003, doi:10.1029/2005SW000193.
- Balsley, B. B. (1973), Electric fields in the equatorial ionosphere: A review of techniques and measurements, *J. Atmos. Terr. Phys.*, *35*, 1035–1044.
- Balsley, B. B., and R. F. Woodman (1969), On the control of the F region drift velocity by the E region electric field: Experimental evidence, *J. Atmos. Terr. Phys.*, *31*, 865–867.
- Bilitza, D. (2001), International Reference Ionosphere 2000, *Radio Sci.*, *36*, 261–275.
- Chau, J. L., and R. F. Woodman (2004), Daytime vertical and zonal velocities from 150-km echoes: Their relevance to F region dynamics, *Geophys. Res. Lett.*, *31*, L17801, doi:10.1029/2004GL020800.
- Fang, T. W., A. D. Richmond, J. Y. Liu, A. Maute, C. H. Lin, and B. Harper (2008a), Model simulation of the equatorial electrojet in the Peruvian and Philippine sectors, *J. Atmos. Sol. Terr. Phys.*, *70*, 2203–2211, doi:10.1016/j.jastp.2008.04.021.
- Fang, T. W., A. D. Richmond, J. Y. Liu, and A. Maute (2008b), Wind dynamo effects on ground magnetic perturbations and vertical drifts, *J. Geophys. Res.*, *113*, A11313, doi:10.1029/2008JA013513.
- Fejer, B. G. (1997), The electrodynamics of the low-latitude ionosphere: Recent results and future challenges, *J. Atmos. Sol. Terr. Phys.*, *59*, 1456–1482.
- Fejer, B. G., D. T. Farley, R. F. Woodman, and C. Calderon (1979), Dependence of equatorial F region vertical drifts on season and solar cycles, *J. Geophys. Res.*, *84*, 5792–5796.
- Fejer, B. G., E. R. de Paula, I. S. Batista, E. Bonelli, and R. F. Woodman (1989), Equatorial F region vertical drifts during solar maxima, *J. Geophys. Res.*, *94*, 12,049–12,054.
- Fejer, B. G., E. R. de Paula, S. A. Gonzales, and R. F. Woodman (1991), Average vertical and zonal F region plasma drifts over Jicamarca, *J. Geophys. Res.*, *96*, 13,901–13,906.
- Fejer, B. G., E. R. de Paula, R. A. Heelis, and W. B. Hanson (1995), Global equatorial ionospheric vertical plasma drifts measured by the AE-E satellite, *J. Geophys. Res.*, *100*, 5769–5776.
- Fejer, B. G., J. W. Jensen, and S. Su (2008), Quiet time equatorial F region vertical model derived from ROCSAT-1 observations, *J. Geophys. Res.*, *113*, A05304, doi:10.1029/2007JA012801.
- Forbes, J. M. (1981), The equatorial electrojet, *Rev. Geophys.*, *19*, 469–504.
- Gagnepain, J., M. Crochet, and A. D. Richmond (1977), Comparison of equatorial electrojet models, *J. Atmos. Terr. Phys.*, *39*, 1119–1124.
- Hedin, A. E. (1991), Extension of the MSIS thermospheric model into the lower and middle atmosphere, *J. Geophys. Res.*, *96*, 1159–1172.
- Hedin, A. E., L. Felming, A. H. Manson, F. J. Schmidlin, S. K. Avery, R. R. Clark, S. J. Fraser, T. Tsuda, F. Vial, and R. A. Vincent (1996), Empirical wind model for the upper, middle, and lower atmosphere, *J. Atmos. Terr. Phys.*, *58*, 1421–1447.
- Hysell, D. L., and J. Burcham (2000), Ionospheric electric field estimates from radar observations of the equatorial electrojet, *J. Geophys. Res.*, *105*, 2443–2460.
- Hysell, D. L., M. F. Larsen, and R. F. Woodman (1997), JULIA radar studies of electric fields in the equatorial electrojet, *Geophys. Res. Lett.*, *24*, 1687–1690.
- Hysell, D. L., J. L. Chau, and C. G. Fesen (2002), Effects of large horizontal winds on the equatorial electrojet, *J. Geophys. Res.*, *107*(A8), 1214, doi:10.1029/2001JA000217.
- Hysell, D. L., J. Chun, and J. L. Chau (2004), Bottom-type scattering layers and equatorial spread F, *Ann. Geophys.*, *22*, 4061–4069.
- Kelley, M. C. (1989), *The Earth's Ionosphere: Plasma Physics and Electrodynamics*, *Int. Geophys. Ser.*, *43*, Academic, San Diego, Calif.
- Maus, S., et al. (2005), The 10th-generation international geomagnetic reference field, *Geophys. J. Int.*, *161*, 561–565, doi:10.1111/j.1365-246X.2005.02641.x.
- Maus, S., E. P. Alken, and H. Luhr (2007), Electric fields and zonal winds in the equatorial ionosphere inferred from CHAMP satellite magnetic measurements, *Geophys. Res. Lett.*, *34*, L23102, doi:10.1029/2007GL030859.
- Nicolet, M. (1953), The collision frequency of electrons in the ionosphere, *J. Atmos. Terr. Phys.*, *3*, 200–211.
- Reddy, C. A., and C. V. Devasia (1981), Height and latitude structure of electric fields and currents due to local east-west winds in the equatorial electrojet, *J. Geophys. Res.*, *86*, 5751–5767.
- Richmond, A. D. (1972), Numerical model of the equatorial electrojet, *Tech. Rep. AFCRL-72-0668*, ERP 421, Air Force Cambridge Res. Lab, Bedford, Mass.
- Richmond, A. D. (1973a), Equatorial electrojet 1: Development of a model including winds and instabilities, *J. Atmos. Terr. Phys.*, *35*, 1083–1103.
- Richmond, A. D. (1973b), Equatorial electrojet 2: Use of the model to study the equatorial ionosphere, *J. Atmos. Terr. Phys.*, *35*, 1105–1118.
- Rush, C. M., and A. D. Richmond (1973), The relationship between the structure of the equatorial anomaly and the strength of the equatorial electrojet, *J. Atmos. Terr. Phys.*, *35*, 1171–1180.
- Shume, E. B. (2006), The equatorial electrojet: Radar observations and modeling, Ph.D. dissertation, Cornell Univ., Ithaca, New York.
- Shume, E. B., D. L. Hysell, and J. L. Chau (2005a), Electron density profiles in the equatorial E region ionosphere derived from a bistatic coherent scatter radar experiment in Perú, *Geophys. Res. Lett.*, *32*, L01107, doi:10.1029/2004GL021715.
- Shume, E. B., D. L. Hysell, and J. L. Chau (2005b), Zonal wind profiles in the equatorial electrojet derived from phase velocities of type II radar echoes, *J. Geophys. Res.*, *110*, A12308, doi:10.1029/2005JA011210.
- Sugiura, M., and D. J. Poros (1969), An improved model equatorial electrojet with a meridional current system, *J. Geophys. Res.*, *74*, 4025–4034.
- Sultan, P. (1996), Linear theory and modeling of the Rayleigh-Taylor instability leading to the occurrence of equatorial spread F, *J. Geophys. Res.*, *101*, 26,875–26,891.
- Woodman, R. F. (1970), Vertical drifts velocities and east-west electric fields at the magnetic equator, *J. Geophys. Res.*, *75*, 6249–6259.

A. Bekele, Department of Physics, Addis Ababa University, P. O. Box 1176, Addis Ababa, Ethiopia.

E. R. de Paula and E. B. Shume, National Institute for Space Research, INPE-DAE, Av dos Astronautas, 1758, Jardim da Granja, 12227-010, São José dos Campos, São Paulo, Brazil. (esayas@dae.inpe.br)

D. L. Hysell, Department of Earth and Atmospheric Sciences, Cornell University, 2108 Snee Hall, Ithaca, NY 14853, USA.
S. Maus, National Geophysical Data Center, NOAA, 325 Broadway, Boulder, CO 80305-3328, USA.

F. S. Rodrigues, Atmospheric and Space Technology Research Associates, 12073 Spectrum Drive, Suite 101, San Antonio, TX 78249, USA.